

Environmental factors driving spatial heterogeneity in desert halophile microbial community

Gherman Uritskiy¹, Adam Munn¹, Micah Dailey¹, Diego R. Gelsinger¹, Samantha Getsin¹, Alfonso F. Davila², P R. McCullough^{3, 4}, James Taylor¹, Jocelyne DiRuggiero^{5*}

¹Biology, Johns Hopkins University, United States, ²Ames Research Center, United States, ³Physics and Astronomy, Johns Hopkins University, United States, ⁴Space Telescope Science Institute (NASA), United States, ⁵Biology and Earth & Planetary Sciences, Johns Hopkins University, United States

Submitted to Journal:
Frontiers in Microbiology

Specialty Section:
Extreme Microbiology

Article type:
Original Research Article

Manuscript ID:
578669

Received on:
30 Jun 2020

Frontiers website link:
www.frontiersin.org

Conflict of interest statement

The authors declare that the research was conducted in the absence of any commercial or financial relationships that could be construed as a potential conflict of interest

Author contribution statement

GU, JT, and JD conceived and oversaw the study; GU, DG, AD, and JD collected in-field samples and metadata; GU, AM, MD, and SG processed field samples and constructed sequencing libraries; PM collected and analyzed light spectra; GU processed and analyzed the data and wrote the manuscript; AD, JT, PM, and JD edited the manuscript.

Keywords

microbiome, extremophile, desert, heterogeneity, Metagenome

Abstract

Word count: 172

Spatial heterogeneity in microbial communities is observed in all natural ecosystems and can stem from both adaptations to local environmental conditions as well as stochastic processes. Extremophile microbial communities inhabiting evaporitic halite nodules (salt rocks) in the Atacama Desert, Chile, are a good model ecosystem for investigating factors leading to microbiome heterogeneity, due to their diverse taxonomic composition and the spatial segregation of individual nodules. We investigated the abiotic factors governing microbiome composition across different spatial scales, allowing for insight into the factors that govern halite colonization from regional desert-wide scales to micro-scales within individual nodules. We found that water availability and community drift account for microbiome assembly differently at different distance scales, with higher rates of cell dispersion at the smaller scales resulting in a more homogenous composition. This trend likely applies to other endoliths, and to non-desert communities, where dispersion between communities is limited. At the intra-nodule scales, a light availability gradient was most important in determining the distribution of microbial taxa despite intermixing by water displacement via capillary action.

Contribution to the field

Understanding the relationship between microbial community composition and environmental factors is key to making robust predictions of microbiome dynamics. In desert ecosystems, water has been identified as the core deterministic factor for microbial community assembly but few studies investigated the relative contributions of deterministic and stochastic factors to community assembly over temporal or spatial scales. In this study, we investigated the abiotic factors governing microbiome compositions from regional desert-wide scales to micro-scales within individual halite nodules (salt rocks). We found that water, light, and community drift impact microbiome assembly differently at different distance scales, with higher rates of cell dispersion at the smaller scales resulting in a more homogeneous composition. This trend likely applies to other endoliths, and to non-desert communities where dispersion between communities is limited.

Funding statement

This work was funded by grants NNX15AP18G and 18-EXO18-0091 from NASA and DEB1556574 from the NSF

Ethics statements

Studies involving animal subjects

Generated Statement: No animal studies are presented in this manuscript.

Studies involving human subjects

Generated Statement: No human studies are presented in this manuscript.

Inclusion of identifiable human data

Generated Statement: No potentially identifiable human images or data is presented in this study.

Data availability statement

Generated Statement: The datasets presented in this study can be found in online repositories. The names of the repository/repositories and accession number(s) can be found below:
<https://www.ncbi.nlm.nih.gov/>, PRJNA641398.

In review

1 **Environmental factors driving spatial heterogeneity in desert halophile**
2 **microbial community**

3
4
5 Gherman Uritskiy¹, Adam Munn¹, Micah Dailey¹, Diego R. Gelsinger¹, Samantha Getsin¹, Alfonso
6 Davila², P. R. McCullough^{3,4}, James Taylor^{1,5}, Jocelyne DiRuggiero^{1,6*}
7
8

9 ¹ Department of Biology, Johns Hopkins University, Baltimore, MD 21218, USA

10 ² NASA Ames Research Center, Moffett Field, CA 94035, USA

11 ³ Department of Physics and Astronomy, Johns Hopkins University, Baltimore, MD 21218, USA

12 ⁴ Space Telescope Science Institute, Baltimore, MD 21218, USA

13 ⁵ Department of Computer Science, Johns Hopkins University, Baltimore, MD 21218, USA

14 ⁶ Department of Earth and Planetary Sciences, Johns Hopkins University, Baltimore, MD 21218,
15 USA

16

17

18 *** Correspondence:**

19 Jocelyne DiRuggiero

20 jdiruggiero@jhu.edu

21

22 **Keywords:** microbiome₁, extremophile₂, desert₃, heterogeneity₄, metagenomes₅.

23 **Abstract**

24

25 Spatial heterogeneity in microbial communities is observed in all natural ecosystems and can stem
26 from both adaptations to local environmental conditions as well as stochastic processes.27 Extremophile microbial communities inhabiting evaporitic halite nodules (salt rocks) in the Atacama
28 Desert, Chile, are a good model ecosystem for investigating factors leading to microbiome
29 heterogeneity, due to their diverse taxonomic composition and the spatial segregation of individual
30 nodules. We investigated the abiotic factors governing microbiome composition across different
31 spatial scales, allowing for insight into the factors that govern halite colonization from regional
32 desert-wide scales to micro-scales within individual nodules. We found that water availability and
33 community drift account for microbiome assembly differently at different distance scales, with higher
34 rates of cell dispersion at the smaller scales resulting in a more homogenous composition. This trend
35 likely applies to other endoliths, and to non-desert communities, where dispersion between
36 communities is limited. At the intra-nodule scales, a light availability gradient was most important in
37 determining the distribution of microbial taxa despite intermixing by water displacement via capillary
38 action.

39

40 Introduction

41 Understanding the relationship between microbial community composition and environmental
42 factors is key to making robust predictions of microbiome dynamics (Green et al., 2008). Factors that
43 limit growth or survival in a given environment will have the largest impact on community assembly
44 (Goldford et al., 2018; Zhao et al., 2019). Many microbial communities are nutrient-limited, meaning
45 that the ability to utilize the available carbon sources is the strongest force of microbial selection
46 (Mello et al., 2016). In extreme environments, however, other factors such as water availability,
47 temperature, pH, or salinity might be more critical (Frossard et al., 2015; Armstrong et al., 2016;
48 Merino et al., 2019), making such systems valuable models for investigating processes influencing
49 microbial community assembly (Schmid et al., 2020). In desert ecosystems, in particular, water has
50 been identified as the core deterministic factor for microbial community assembly (Crits-Christoph
51 et al., 2013; Merino et al., 2019; Uritskiy et al., 2019a). However, few studies investigated the
52 relative contributions of deterministic and stochastic (i.e. non-random and random) factors to
53 community assembly over temporal or spatial scales (Caruso et al., 2011; Feeser et al., 2018).

54 Comparative microbiome studies in the Atacama Desert, Chile, provide valuable insight into
55 factors impacting community assembly because of humidity and temperature gradients and unique
56 geological features across the desert (Cáceres et al., 2007). Microbial communities living inside
57 halite nodules (NaCl rocks) are of particular interest due to their diverse taxonomic composition and
58 spatial segregation (Wierzchos et al., 2006; Davila et al., 2015). Isolated inside individual nodules,
59 these diverse communities develop largely independently from one another due to minimal exchange
60 of biomass and nutrients (Crits-Christoph et al., 2016; Uritskiy et al., 2019a). Despite an average
61 annual precipitation of less than 1 mm, microbial life in these microbiomes have evolved to rely on
62 changes in air relative humidity (RH) (Davila et al., 2008; Davila et al., 2015). Facing extremely dry
63 conditions causes their composition to be particularly sensitive to changes in the environment,
64 making them a compelling model to investigate the early effects of climate change on microbiome
65 composition and function (Uritskiy et al., 2019a).

66 The deliquescent properties of NaCl allow it to draw on moisture from the air above 75% RH,
67 producing small amounts of liquid brine in the interior of halite nodules, which support halite
68 communities in the driest parts of the Atacama Desert (Wierzchos et al., 2012; Davila et al., 2020). In
69 some locations, the proximity of the ocean and the presence of unique wind patterns result in high
70 RH swings during the diel cycle – from 30% during the day to 90% during the night (Cereceda et al.,
71 2008; Finstad et al., 2016). As the halite nodules dehydrate during the day, capillary action moves

72 brine toward the surface, resulting in an overall displacement of salt, organic molecules, and possibly
73 even live cells (Davila et al., 2008; Davila et al., 2013).

74 Because of the saturated salt conditions, the halite microbial communities are comprised of
75 highly adapted halophiles (Robinson et al., 2015; Crits-Christoph et al., 2016; Finstad et al., 2017).
76 The two dominant heterotrophic taxa found in this community are halophilic *Halobacteria* (members
77 of the *Euryarchaeota*) and *Salinibacter* (members of the *Bacteroidetes*). These halophiles are salt-in
78 strategists, meaning they import potassium ions to counteract the external osmotic pressure from
79 sodium ions (Oren, 2008; Gunde-Cimerman et al., 2018). Other heterotrophs in the community
80 include halophilic *Proteobacteria*, *Actinobacteria*, and *Nanohaloarchaea* – an ectoparasite of
81 *Halobacteria* (Crits-Christoph et al., 2016; Hamm et al., 2019). The biologically available carbon in
82 the community is fixed by several species of *Cyanobacteria* and a single green alga (Finstad et al.,
83 2017; Uritskiy et al., 2019b). Previous characterization of the community metatranscriptome revealed
84 that all the major community members are transcriptionally active (Uritskiy et al., 2019b; Gelsinger
85 et al., 2020), with photosynthesis and carbon fixation being highly prioritized in the transcriptomes of
86 photoautotrophs. Additionally, *Halobacteria* and *Salinibacter* enhanced the transcription of
87 bacteriorhodopsins and xanthorhodopsin, respectively; those are modified rhodopsins that in the
88 presence of light are used to form a proton gradient and thus generate ATP (Oren, 2014; Seyedkarimi
89 et al., 2015).

90 Previous research into halite microbial community heterogeneity reported that changes in the
91 composition of halite microbiomes over regional distance scales (tens of kilometers) were linked to
92 moisture availability (Robinson et al., 2015; Finstad et al., 2017), although the widespread
93 distribution of a specific *Cyanobacteria* suggested inter-site dispersal along a moisture gradient
94 (Finstad et al., 2017). One important question remains, what is the distribution of the halite
95 community within a nodule? Our study builds on previous findings and focuses on local distance
96 scales to investigate the deterministic and stochastic forces influencing the halite microbial
97 community at the meter and centimeter distance scales.

98

99 **Materials and Methods**100 **Sampling scheme and scales of diversity**

101 Regional distance scales were investigated by sampling the North and the South ends of Salar
102 Grande, a salar located in the Northern part of the Atacama Desert (Robinson et al., 2015) (Fig. 1).
103 Samples of halite nodules were collected from 500m² areas at each end of the salar, with 39 samples
104 from the North site and 46 samples from the South site (Supp. Data 1). The North and South regions
105 were 19km apart and were at a similar distance to the Pacific Ocean (11.6km for the North site and
106 9.9km for South site). However, the height of the Coastal Mountain Range separating the salar from
107 the Ocean was significantly different, with 450m-804m above salar level in the North and 58m-205m
108 above salar level in the South. A hill at the North location was used for comparing halite microbiome
109 composition at landscape distance scales. The hill had 32m of elevation gain over 330m. On Feb 2,
110 2016, 19 samples were collected from the top of the hill, and 12 from the bottom. In both sampling
111 locations, nodules were collected in 20m² regions (Supp. Data 1). For the local distance scale, we
112 performed a more detailed sampling of 6 halite nodules collected in a 10m² area at the top of the
113 North hill on Feb 20, 2018. These nodules were vertically sliced with a mechanical saw two times,
114 separating them into three pieces. In each slice, the top, middle, and bottom sampling locations were
115 determined by selecting three equidistant positions along the vertical axis (Supp. Data 1). Due to the
116 high number of samples, we harvested nodules for the different spatial scales on different dates
117 (Supp. Data 1), however, all direct comparisons were performed between samples collected at the
118 same scale and on the same date. In the field, halite nodules were harvested by breaking them open
119 with a sterilized hammer and collecting colonized pieces (1-10cm across) from the center of the
120 nodules in sterile Whirl-pack bags. Nodule pieces were stored in dark in dry conditions for up to 8
121 weeks, until further processing. Entire nodules were also wrapped in plastic, transported to the lab,
122 and stored in similar conditions.

123

124 **Environmental conditions**

125 Landscape- and regional-scale atmospheric relative humidity (RH) and temperature (T) conditions
126 were recorded for one year with HOBO Pro v2 External T/RH Data Loggers installed 1 meter above
127 the ground at each of the sampling locations. RH and T data were used to estimate the occurrence
128 frequency and average duration of dew (when RH>95%) and fog (when RH>99%) events at each site.
129 Intra-nodule RH and T conditions were recorded for one year with the same sensors installed inside

130 three representative halite nodules within a 10 m² area at the North-Top location. Probes were installed
131 in the top, center, and bottom of the halite by drilling holes in close proximity to the desired position,
132 inserting the probe, and sealing the hole back with a commercial resin. In all cases, the data loggers
133 were set to record measurements every 30 minutes.

134

135 **Light transmission measurements inside halite nodules**

136 Light transmission in the top, middle and bottom of halite nodules was measured with an Ocean
137 Optics Flame-S-XR1 spectrometer (Ocean Optics, Largo, FL) with a range of 220-1025 nm and
138 equipped with a 25µm slit and a 600 µm optical fiber probe, as previously reported (Meslier et al.,
139 2018). In short, halite nodules were placed under controlled lighting conditions with a broad-
140 spectrum 500 W halogen lamp 44 cm above the nodule as the only source of illumination. The
141 optical fiber probe, equipped with a cosine corrector to homogenize the fiber optic cable's angular
142 response, was inserted into a tight hole drilled in the underside of the halite nodule to the desired
143 distance from the top. The relative effective light transmission at each wavelength was estimated by
144 dividing each measurement to the respective intensity measured from the unfiltered light source (the
145 broad-spectrum lamp). The lamp's spectrum was measured and used for normalization of the data to
146 obtain the effective transmission inside the halite, thus nullifying any major differences between the
147 spectra from the lamp and the sun. Only 500nm – 900nm wavelengths were considered. To account
148 for inter-halite variability in the comparison of light transmittance to the top and middle positions of
149 the halite nodules, the light transmittance measurements were standardized to the mean of the “top”
150 measurements made in all three nodules. For the bottom positions within the nodules, we found that
151 our direct transmission measurements in the lab could not reproduce realistic conditions from the
152 desert, as light in the field scattered around and even underneath the halite nodules. The transmission
153 measurements made at the top and middle positions inside the halite nodules were used with that of
154 the unobstructed solar light to approximately estimate the photosynthetically active radiation (PAR)
155 available inside the nodules. For each intra-nodule measurement, the area under the transmission
156 curve was calculated in the 400 µm -700 µm range, and this value was divided by that of the solar
157 transmission spectrum to get the effective PAR reduction ratio. Because of the relatively uniform
158 solar transmission spectrum in this range, this reduction ratio could be multiplied by the maximum
159 observed solar PAR during midday at the sampling location (measured at 2100 µmol/m²/sec) to
160 obtain the approximate PAR available inside the nodules. It is important to note that the true PAR
161 available inside the halite nodules might be somewhat higher than these estimates due to light
162 scattering from all directions inside the pores, and additional light scattering from the sides of the

163 nodule. To address this, an additional experiment using the same experimental set up was carried out
164 using homogeneous 9cm x 9cm x 6 cm (tall) blocks of salt (American Stockman white salt, Compass
165 Minerals, Overland Park, KS). The salt block's periphery was wrapped in aluminum foil to
166 approximate an infinite slab of illuminated brick. Spectra were taken with the optic fiber probe aimed
167 upward from a hole drilled from below and compared with spectra taken with the probe aimed
168 downward in a hole at the same location in the block.

169

170 **DNA extraction**

171 Colonized halite pieces were ground into fine powder as previously described (Robinson et al.,
172 2015). For intra-halite sampling, six intact nodules were vertically sliced with a mechanical saw as
173 described above, exposing the colonization areas within. The interiors of the nodules were then
174 scraped with a sterile knife to obtain sufficient material (2 g) and the distance to the nodule's surface
175 was recorded (Fig. 1D). Cells were extracted from the ground halite powder as previously described
176 (Robinson et al., 2015; Urtskiy et al., 2019a) and the DNAeasy Powersoil DNA extraction kit
177 (QIAGEN) was used to extract gDNA from the resulting cell pellet.

178

179 **DAPI cell count**

180 Total biomass in halite samples was estimated by fluorescence microscopy cell counting (Kepner and
181 Pratt, 1994) using 0.5 g of ground halite. The halite powder was gradually dissolved in a solution of
182 20% NaCl, 1% TWEEN. The solution was gently shaken for 30 minutes to break cell clumps and
183 DAPI was added to a final concentration of 0.5 µg/ml. After a 10-min incubation, 2 ml of the
184 solution were filtered on a 25 mm diameter black polycarbonate filter (3 filter replicates in total).
185 Filters were imaged using a DAPI (blue) fluorescent light filter at 400x magnification on a Zeiss
186 *Imager.A1* microscope with an *X-Site series 120* fluorescence lamp illuminator. For each filter, 5
187 images were taken with a *Zeiss AxioCam MRm* black-and-white camera (15 images total for each
188 halite sample; minimum field-of-view cell count was 35 cells and the mean was 364 cells). The total
189 number of visible cells was counted in each image using an automate *CellProfiler* v2.1 pipeline, in
190 which the *CorrectIlluminationCalculate* function was used to normalize the background light levels,
191 and *IdentifyPrimaryObjects* function was used to find and count unique nuclei (see Supp. Data 2 for
192 parameters). The number of cells per gram of halite was calculated from the number of cells in each
193 image and taking into account the *eFOV* of the camera at that magnification (0.203 mm²), the total
194 area of the filter (226.98 mm²), and the amount of halite powder. To get a more robust cell count

195 estimate in each biological replicate, 3 technical replicates were performed for each sample, and 5
196 fields of view were counted per technical replicate. Among the 15 cell count replicates for each
197 biological replicate, replicates with estimates outside of 2 standard deviations of the mean were
198 discarded.

199

200 **16S rRNA gene amplicon library preparation and sequencing**

201 The 16S rRNA gene was amplified from gDNA using a 2-step amplification and barcoding PCR
202 strategy, and primers 515F and 926R primers for the hypervariable V3-V4 region, as previously
203 described (Needham and Fuhrman, 2016; Urtskiy et al., 2019a). PCR was done with the Phusion
204 High-Fidelity PCR kit (New England BioLabs), the barcoded amplicons were quantified with the
205 Qubit dsDNA HS Assay Kit (Invitrogen), pooled, and sequenced on the Illumina MiSeq platform
206 with 250 bp paired-end reads at the Johns Hopkins Genetic Resources Core Facility (GRCF).

207

208 **16S rRNA gene amplicon sequence variant pre-processing**

209 The de-multiplexed and quality trimmed 16S rRNA gene amplicon reads from the sequencer were
210 processed with Qiime2 2018.8.0 (Bolyen et al., 2019a). The major comparison experiments (regional,
211 landscape, and local distance scales) were processed independently. Dada2 (Callahan et al., 2016)
212 was used to call amplicon sequence variants (ASVs) using only the forward reads of the amplicon
213 data (options: --denoise-single, --p-trunc-len 230 --p-chimera-method consensus). Alignment mafft
214 was used to create a multiple alignment of ASV sequences and phylogeny fasttree was used to
215 construct the phylogeny tree. The sampling depth used for the core-metrics-phylogenetic generation
216 was chosen independently in each experiment based on the sample with the lowest read coverage.
217 For ASV taxonomy assignment, a feature-classifier was first built using the SILVA 16S rRNA gene
218 v128 database (Quast et al., 2013) and the sequence of the 515F universal primer.

219

220 **Controls and replication**

221 Three samples from the top of the hill at the North sampling site were extracted twice to estimate the
222 dissimilarity between biological replicates collected from the same original halite nodule powder
223 sample. The corresponding six sequencing libraries were processed and sequenced the same way as
224 the other samples in this study but sequenced on a separate run. Qiime2 beta-diversity estimation was

225 used to estimate the average Weighted Unifrac dissimilarity between biological replicates: 0.105 +/-
226 0.015.

227

228 **Statistical comparisons of community compositions at different sites**

229 All comparisons between sites were made with built-in statistical packages within Qiime2 2018.8.0
230 (Bolyen et al., 2019b). Alpha and beta-diversity metrics were calculated for each distance scale
231 experiment by using the core-metrics-phylogenetic command. Alpha diversity between different
232 sample groups was compared with the alpha-group-significance with both the PD and Evenness
233 diversity metrics, and the significance between beta diversity between sites was computed with the
234 beta-group-significance command using the Weighted Unifrac dissimilarity matrices (Tucker et al.,
235 2017). The PCoA projection of the Weighted Unifrac dissimilarity matrices was imported into
236 custom visualization scripts. Enrichment for specific taxa at each taxonomic rank was tested using
237 the ANCOM statistical enrichment test (Mandal et al., 2015). The taxonomy of each ASV was
238 estimated with the classify-sklearn command using a custom classifier (as described above), and the
239 relative abundance of major taxonomic groups was imported into custom scripts for plotting and
240 statistical analysis. Differential abundance significance of each taxon was tested using an
241 independent two-sided T-test. For the intra-halite sample comparison, the relative abundances were
242 also standardized to account for high inter-nodule and inter-slice variability. The relative abundance
243 of each taxon in each sample was standardized to its average relative abundance in that slice. The
244 correlation of these normalized abundances with the distance to the nodule surface was calculated
245 with a paired sample two-sided T-test and fitted to a non-parametric regression with the
246 SpatialAverage method in pyqt_fit.

247

248 **Results**249 **Sampling scheme for investigating different scales of diversity**

250 We conducted a robust sampling survey of halite nodules in Salar Grande located in the Atacama
251 Desert, Chile. The community composition and structure were interrogated across four spatial scales
252 ranging from major regions of the salar to micro-niches within a single halite nodule (Table 1; Fig.
253 1). Regional distance scales were investigated by sampling the North and the South ends of Salar
254 Grande (Fig. 1A). The landscape distance scale was investigated along a hill at the North location,
255 which had a 32m of elevation gain over 330m (Fig. 1B). For the local distance scales, we performed
256 a more detailed sampling of 6 halite nodules from the top of the North hill (Fig. 1C, D).

257

258 **Differences in temperature, relative humidity, and light availability across spatial scales**

259 Climate conditions in the North and South sites were significantly different. During the tested period,
260 the South site was consistently cooler (by 5.2°C on average; Fig. S1A) and more humid (by 11% RH
261 on average; Fig. S1B) than the North. These differences were minimal during the night and early
262 morning. After coastal winds picked up around noon, the differences in temperature and atmospheric
263 RH began to increase, with the greatest differences at ~ 2 pm, with changes as high as 7 °C and 15%
264 for temperature and RH, respectively. Air sensors at the South site recorded 147 days with dew
265 formation (average duration: 3 hours; maximum duration: 9.5 hours) and 31 days with fog formation
266 (average duration: 9 hours; maximum duration: 15.5 hours). Air sensors at the North site recorded 66
267 days with dew formation (average duration: 2 hours; maximum duration: 9.5 hours) and 15 days with
268 fog formation (average duration: 6.4 hours; maximum duration: 11 hours).

269 At the landscape scale (North-top and North-bottom) there were small differences in
270 temperature and significant differences in moisture conditions. Specifically, the hilltop was
271 somewhat cooler (2-3 °C; Fig. S1C) and more humid (3-7%; Fig S1D) during the morning hours.
272 Sensors at the hilltop site recorded 85 dew days (average duration: 2.1 hours; maximum duration: 8
273 hours) and 20 fog days (average duration: 7.1 hours; maximum duration: 11 hours), whereas sensors
274 at the hill bottom site recorded 47 dew days (average duration: 2 hours; maximum duration: 6 hours)
275 and 10 fog days (average duration: 5.7 hours; maximum duration: 8 hours).

276 The interior temperature of the halite closely tracked that of the outside air, with the
277 temperatures near the surface of the halite sometimes reaching as high as 40 °C (Fig. 2A-C). The RH
278 inside the halite nodule was notably higher than the surrounding air (Fig. 2D-E), particularly during

279 the day, when the atmospheric RH dropped significantly to as low as 20%, while the internal nodule
280 RH never dropped below 75%. These results were reproducible across 3 replicate halite nodules
281 measured at the North location. These internal nodule condition measurements were recorded one
282 year after the intra-nodule sampling took place, however, the atmospheric temperature and RH
283 conditions were very similar between the two years (Fig. S2).

284 A fiber optic spectrometer was used to measure transmission spectra at the top and middle
285 positions within the halite nodules (Fig. S3). These spectra, together with the photosynthetically
286 active radiation (PAR) of sunlight at its midday maximum of $2100 \mu\text{mol}/\text{m}^2/\text{sec} +/- 105$, as measured
287 with a commercial Hobo meter, were used to estimate the average available PAR in the top- ($4.70 \mu\text{mol}/\text{m}^2/\text{sec} +/- 1.07$) and middle-position ($0.11 \mu\text{mol}/\text{m}^2/\text{sec} +/- 0.06$) with the halite nodules. The
288 difference in available light for photosynthesis was even greater in the primary excitation wavelength
289 of chlorophyll *a* (680nm), with the center of the nodules receiving as little as 1% of the light usable
290 for photosynthesis at this wavelength compared to that of the top of the nodule. To determine
291 whether the light was approximately isotropic inside the halite nodules, transmission spectra were
292 taking using homogenous salt blocks with the fiber optic probe positioned looking toward or away
293 from the incident light. The light intensity inside the salt block measured with the probe aimed
294 downward (away from the incident light) was typically 30% of the intensity at the same location but
295 with the probe aimed upward (toward the incident light), indicating that a small correction factor of
296 1.3 may be applied to the measurements in halite nodules.
297

298

299 **Biomass distribution inside halite nodules**

300 As an estimate for total biomass, cell numbers per g of substrate were counted for a subset of nodules
301 at the top, middle, and bottom positions. Each nodule was sliced vertically in two locations, and the
302 top, middle, and bottom (approximately equidistant) positions in each slice were sampled. A semi-
303 automated DAPI cell counting assay was used to count the number of cells per field of view under a
304 microscope, and then back-calculate cell number per gram of halite material at each sampled
305 location. We found a great degree of biomass variability between halite nodules, as well as between
306 slices from the same nodule, ranging from 0.5×10^6 to 9×10^6 cells per gram of ground halite (Fig. S4).
307 To account for this variation in biomass between slices, the average cell count estimates of each
308 biological replicate were standardized to the maximum value in that slice (Fig. S5). Doing so
309 revealed that there was no position in the nodules that had predictably higher or lower biomass. Out
310 of the 12 slices interrogated, 2 had the highest biomass at the top, 4 at the middle, and 6 at the
311 bottom.

312

313 **Microbial community structure diversity across different distance scales**

314 We compared the microbial community composition between sampling sites by clustering 16S rRNA
315 gene sequences at the amplicon sequence variant (ASV) level and by comparing each pair of samples
316 with the Weighted Unifrac dissimilarity index, a diversity metric that measures the dissimilarity in
317 ASV composition while accounting for ASV phylogenetic similarity. The dissimilarity matrix,
318 resulting from this analysis, was then used to compute differences between sampling locations for all
319 spatial scales. At the regional (North vs. South) and landscape (North-top vs North-bottom) distance
320 scales, we found the microbial community composition to be significantly different between sites
321 (*PERMANOVA*: $pval < 0.001$; Fig. 3A, B). We also found that the average inter-sample dissimilarity
322 between the North and the South was higher than that between North-top and North-bottom (0.96 and
323 0.91, respectively; Student's T-test, $pval < 0.001$).

324 A closer look inside neighboring nodules at the North-top sampling site revealed substantial
325 diversity in microbial community composition inside the nodules (Figs. 3 and S6). Collected samples
326 differed significantly between nodules, between slices, and between the top, middle, and bottom
327 positions of different nodules (*PERMANOVA*: $pval < 0.01$). While these differences were statistically
328 significant, principal coordinate analysis showed these samples only weakly separated along the first
329 and second principal components by nodule and slice identifiers (Fig. S6). The top-middle-bottom
330 spatial separation was only evident along the third and fourth principal components (Fig. 3C, D). The
331 first and second principal components explained a much greater degree of inter-sample variability
332 (49% and 11%, respectively) compared to that of the third and fourth components (7% and 6%,
333 respectively), suggesting that more differential ASV features were linked to the slice and nodule
334 identifiers rather than vertical positioning within the nodules.

335

336 **Differences in phyla relative abundances across the distance scales**

337 To investigate the underlying reasons for the observed differences in microbial community structure
338 between the sampled locations, we compared the relative abundance compositions at the phylum
339 level. As previously reported, the 6 most abundant phyla in halite nodule microbial communities
340 were *Euryarchaeota* (almost exclusively comprised of *Halobacteria*), *Bacteroidetes* (primarily
341 *Salinibacter*), *Cyanobacteria*, *Proteobacteria*, *Actinobacteria*, *Nanohaloarchaea*, and in some cases
342 a green alga (*Dolichomastix spp.*) (Crits-Christoph et al., 2016; Urtskiy et al., 2019b).

343 Focusing on these taxa, we found that the taxonomic compositions at the North and South
344 sites of the salar differed significantly (Fig. 4A, S7A), despite the high composition variability
345 introduced by sampling over broad areas of the salar ($\sim 500\text{m}^2$). On average, the relative abundance of
346 *Euryarchaeota*, which constituted the majority of the community at both locations, was higher at the
347 North location while the relative abundances of *Chlorophyta* and *Proteobacteria* were higher at the
348 South location and were almost absent in the North (Student T-tests, $p\text{val}<0.0001$). Unexpectedly, we
349 found that the *Chlorophyta* (the alga's chloroplast) 16S rRNA gene relative abundances in the South
350 were nearly equal and sometimes greater than that of *Cyanobacteria*. Evaluating taxon differences
351 with the analysis of the composition of microbiomes (ANCOM) enrichment test also revealed similar
352 trends (Fig. 4A). ANCOM is a differential abundance method that aims to produce few false-
353 positives by not making any assumptions about the distribution and structure of the underlying data,
354 and uses a W-statistic to represent the number of features that a single feature is tested to be
355 significantly different against (Mandal et al., 2015). At the class level, *Chlorophyta* and
356 *Gammaproteobacteria* were more relatively abundant in the South (ANCOM $W=20$ and 18 ,
357 respectively). *Cyanobacteria*, on the other hand, were significantly more relatively abundant at the
358 North location (ANCOM $W=18$). At the domain level, archaea (which were largely comprised of
359 *Euryarchaeota*) were significantly more relatively abundant in the North (ANCOM, $W=2$).

360 Comparing the relative taxonomic composition of halite microbial communities at the top and
361 bottom of the North hill also revealed major differences in phyla abundances (Fig. 4B, S7B). These
362 samples were collected within 20m^2 areas at the top and bottom, so the inter-replicate composition
363 variability was notably lower than that between samples collected over larger areas. *Cyanobacteria*
364 were relatively more abundant at the bottom of the hill than at the top (Student T-test $p\text{val}<0.001$),
365 while *Euryarchaeota*, *Proteobacteria*, and *Actinobacteria* were more abundant at the top (Student T-
366 test $p\text{val}<0.0001$). *Chlorophyta* chloroplast sequences were only detected at low abundances in a few
367 samples at the bottom and top, resulting in inconclusive statistical comparison. Evaluating taxa
368 enrichment with the ANCOM significance test produced slightly different results than that from the
369 T-tests on the total relative phyla abundances, specifically in the interpretation of the
370 *Nanohaloarchaea* and *Euryarchaeota* relative abundance differences (Fig. 4B). *Nanohaloarchaea*
371 (which was not identified as differentially abundant by the T-test), *Proteobacteria*, and
372 *Actinobacteria* were found to be significantly more relatively abundant at the top of the hill than the
373 bottom (ANCOM $W=6,9,8$, respectively), and *Cyanobacteria* was more relatively abundant at the
374 bottom of the hill (ANCOM $W=7$). No ANCOM significance in relative abundance was observed for
375 *Euryarchaeota*, although it was significant in the T-test analysis.

376 Next, we investigated the diversity in phylum-level relative composition in different positions
377 (top, middle, bottom) of the halite nodule interiors. Because of the high inter-nodule and inter-slice
378 variability of the microbial community composition, the relative abundance of each taxon in each
379 sample was standardized to its average relative abundance in that slice. This standardization resulted
380 in a relative abundance average of 1 and highlighted differences in phyla spatial distribution along
381 the top, middle, and bottom position of the nodules (Fig. S8). We found that *Euryarchaeota*
382 (constituted entirely of *Halobacteria*) was more relatively abundant at the bottom of the halite than
383 the middle, while *Bacteroidetes* showed the reverse trend, being more relatively abundant in the
384 middle than the bottom (Student's T-test, $pval < 0.01$; Fig. 5). However, the magnitudes of these
385 differences were small (<8% and <20%, respectively). *Cyanobacteria* were significantly and
386 consistently more relatively abundant by more than 80% at the tops of the nodules than the middles
387 (Student's T-test, $pval < 0.001$). *Actinobacteria*, *Nanohaloarchaea*, and *Proteobacteria* were
388 consistently more relatively abundant in the middle of the halite nodules and less relatively abundant
389 at the top and bottom positions (Student's T-test, $pval < 0.01$). This preference for the center of the
390 nodules resulted in a major increase in relative abundance at the center compared to the top and
391 bottom positions of ~310% for *Actinobacteria*, ~70% for *Nanohaloarchaea*, and ~50% for
392 *Proteobacteria*. *Chlorophyta* (chloroplast) sequences were only detected at low relative abundances
393 in a few samples, and thus were not included in this analysis.

394 We also correlated the community composition to the shortest distance of each sampling
395 location to the surface of the nodule (either top or bottom), which confirmed preferences of some
396 taxa towards the nodule interior versus the exterior (Fig. S8). Just as described above, the abundances
397 of each taxon in each position were standardized to their average abundance in each slice. The
398 significance of the positive and negative trends was evaluated with a Spearman correlation test as
399 well as a two-sided paired T-test ($pval < 0.01$). Similar to what was found in the categorical
400 comparisons, *Actinobacteria*, *Nanohaloarchaea*, and *Proteobacteria* were significantly more
401 relatively abundant further away from the surface, reaching maximum relative abundances at 2-3cm
402 away from the nodule surface. *Cyanobacteria* on the other hand, significantly decreased in relative
403 abundance as the distance to the surface increased. Interestingly, both *Euryarchaeota* and
404 *Bacteroidetes* relative abundances were not significantly correlated with the distance to the surface.
405

406 Water availability dictates community diversity

407 To investigate the effects of environmental factors on community diversity, we analyzed the
408 microbial alpha diversity between sampling locations. Comparing alpha diversity metrics across the

409 regional and landscape scales of diversity at the ASV level revealed that the phylogenetic diversity
410 was generally higher in the more humid locations (Table S1). Communities from samples collected at
411 the South site had significantly higher Faith Phylogenetic Diversity (Faith PD) than those from the
412 North (Kruskal-Wallis, $pval < 0.001$), while the Simpson and Shannon diversity indexes were not
413 significantly different. Samples from the top of the North hill were more diverse than those at the
414 bottom in terms of Faith PD, Shannon, and Simpson alpha diversity indexes (Kruskal-Wallis,
415 $pval < 0.01$). In contrast, at the local distance scales (intra-halite), measures of alpha diversity did not
416 yield significant differences with categorical tests, however, a paired statistical test revealed that the
417 center position within the halite nodules generally had higher taxonomic diversity than the top (two-
418 sided paired t-test, $pval < 0.01$). The other position pairings did not show a significant difference in
419 alpha diversity (Table S2).

420

421 **Community structure becomes more similar with increased physical proximity**

422 Inter-sample dissimilarity comparisons were also used to determine whether samples collected farther
423 apart (regional distance scales) were more dissimilar than those collected closer together (smaller
424 distance scales). Comparing average Weighted Unifrac dissimilarities between locations revealed that
425 the average inter-sample dissimilarity was the highest at the largest distance scales, but became
426 significantly smaller as samples became closer (Fig. S9). Performing the same analysis by using the
427 Bray-Curtis dissimilarity metric, which highlights raw community composition differences without
428 considering inter-ASV phylogenetic similarity, revealed an even better resolved dissimilarity
429 differences at the tested distance scales (Fig. 6). With this metric, we found that samples coming
430 from the same positions within the halite nodules (e.g. top positions of halite 1) were more similar
431 than those coming from different positions (Student's T-tests, $pval < 0.001$). In general, the inter-
432 sample dissimilarity had a significant positive correlation with increasing distance.

433

434

435 Discussion

436 Our detailed sampling of the halite nodule community composition across spatial scales allowed us to
437 investigate the factors governing community assembly at each scale of diversity. Across all
438 investigated distance scales, we found that the composition of the halite microbial communities
439 became more similar the closer they were to one another. This finding is consistent with a previous
440 investigation of halite microbiome diversity, where communities were more similar at the landscape
441 distance scale compared to the regional distance scale (Finstad et al., 2017). This trend could be
442 explained, in part, by dispersion limitation, resulting in geographic isolation and producing different
443 community composition outcomes over time. Indeed, contained in rocks, the halite microbial
444 communities have limited capacity to disperse, and increased distances make this even less likely.
445 These divergent outcomes, in a process called ecological drift, are the result of stochastic
446 composition fluctuations (Nemergut et al., 2013; Evans et al., 2017). Therefore, the observed
447 community composition differences are likely indicative of community ecological drift, particularly
448 at the regional distance scales where stochastic processes relating to randomized initial colonization
449 from the seed bank (Finstad et al., 2017) can be major driving factors for community assembly
450 (Rocha, 2018). These factors likely become less important when considering the intra-nodule
451 distance scales where dispersion becomes less limited, as discussed below.

452 Deterministic factors may also play a role in shaping the halite microbial communities. Our
453 findings showed that relatively small changes in water availability have significant implications for
454 microbial community structure inside halite nodules. Indeed, seemingly minor differences in
455 atmospheric RH had significant impacts on the composition and diversity of microbial communities.
456 Previous research on halite nodule community temporal dynamics demonstrated that the
457 deliquescence of salt is tightly linked with metabolic functions, such as photosynthesis, in the halite
458 microbiomes (Davila et al., 2013). Lack of dispersion between halite nodules coupled with local
459 variations in environmental conditions appear to be sufficient to cause a divergence in community
460 structure even at distance scales of ~10 m.

461 Investigating the difference in the relative abundance of the major halite microbiome phyla
462 across regional and landscape distance scales revealed that *Nanohaloarchaea*, *Proteobacteria*, and
463 *Actinobacteria* were more relatively abundant in locations with higher water availability and more
464 frequent dew and fog formation. These taxa were also consistently more abundant in the nodule
465 centers, indicating that the nodule periphery had less favorable conditions for taxa requiring
466 consistent water availability. While dehydration events inside the nodules were not observed during
467 the study, the RH in the periphery of the nodules can drop below 75% during periods of prolonged
468 dry conditions (J. DiRuggiero, pers. com). *Nanohaloarchaea*, *Proteobacteria*, and *Actinobacteria* are

extremophilic and capable of surviving long-term desiccation (Crits-Christoph et al., 2016), however, these heterotrophs are possibly less adapted than *Halobacteria* and *Bacteroidetes* to survive intermittent desiccation. Under high salt, the salt-in strategy deployed by *Halobacteria* and *Bacteroidetes* is bio-energetically more favorable than the salt-out strategy used by other halophiles (Oren, 2008; Sigliocco et al., 2011) and could translate into a competitive advantage for surviving low water availability at saturated salt conditions. Indeed, these two phyla were more consistently abundant and diverse across regional and landscape scales of diversity. *Nanohalobacteria* are also salt-in strategists, however, they are parasitic and rely strongly on their *Halobacteria* hosts (Hamm et al., 2019). Their adaptations to a parasitic lifestyle include a small cell size and a compact and streamlined genome, both of which could diminish their adaptation to desiccation (Narasingarao et al., 2012; Crits-Christoph et al., 2016). This is consistent with a previous study investigating halite microbiome composition across regions of the Atacama Desert, where *Nanohaloarchaea* was consistently found in the more humid sampled locations (Finstad et al., 2017), and a longitudinal study showing that *Nanohaloarchaea* was less tolerant to the osmotic stress from a rare rainfall than the other taxa (Uritskiy et al., 2019a). While ecological drift could explain some of the differences in the halite community structure on regional and landscape scales, the consistent presence of certain phyla (particularly *Proteobacteria*) at the more humid locations across all scales of diversity points to water availability being the major driving factor in community assembly. This is also supported by our observations of increased alpha diversity in the microbial communities at the more humid sampling sites with more frequent dew and fog events. This is not surprising since water availability has been linked to increasing community complexity, particularly in water-limited ecosystems such as desert microbiomes (Crits-Christoph et al., 2013; Mandakovic et al., 2018), and halite nodule microbiomes in particular (Robinson et al., 2015).

Cyanobacteria was the only phylum that was more relatively abundant in the dryer sites of the salar. This is consistent with previous research across multiple salars of the Atacama Desert, where *Cyanobacteria* were found to be more relatively abundant in halite nodules of the driest salars (Robinson et al., 2015). Inside the halite interior, *Cyanobacteria* were more relatively abundant at the top of the nodules, which aligns with our light transmittance measurements showing that there was more light available for photosynthesis at the tops than at the center of the nodules. Microbial compartmentalization along the vertical axis in response to a light gradient has been well studied in microbial mats, where it was shown that phototrophic bacteria have a consistently higher relative abundance in the surface layers of the mats (Carreira et al., 2015; Nishida et al., 2018). As the light traveled deeper into the nodule, less light was available for photosynthesis, particularly at the 680nm wavelength – the main absorbance wavelength for chlorophyll *a*. Our estimates of available PAR

503 within the nodule interiors ranged from ~5 $\mu\text{mol/m}^2/\text{s}$ near the top surfaces of the nodules to as little
504 as ~0.1 $\mu\text{mol/m}^2/\text{s}$ deep in the nodule interior, although more light could possibly reach deeper areas
505 via vertical channel-like pores present in many nodules (see Fig. 1D). Our PAR calculations are in
506 agreement with previous experimental (Wierzchos et al., 2015) and theoretical (Nienow et al., 1988)
507 estimates of available light in other endolithic environments.

508 The other oxygenic phototroph in halite microbiomes, the green alga, has been characterized
509 with metagenomics and metatranscriptomics in the North location (Uritskiy et al., 2019b), however,
510 our amplicon-based methods detected very low abundances at this site. In contrast, algae were very
511 abundant at the more humid South sampling location. Previous research on these algae has shown
512 that their relative abundance correlated with fog events (Robinson et al., 2015) and also increased
513 after rain events (Uritskiy et al., 2019a), making the increased water availability in the South a likely
514 explanation for their high abundances. *Halobacteria* and *Salinibacter* can also use light via microbial
515 rhodopsins, which are light-driven proton pumps allowing them to produce chemical energy. These
516 two taxa were found to be evenly distributed within the halite interior.

517 We found no consistent trend in the total number of cells at the top, middle, and bottom
518 sections of halite nodules. While this was surprising considering the differences in light flux at these
519 positions, these findings are also consistent with previous reports of cell numbers at different
520 positions within halite nodules (Finstad et al., 2017). The seemingly random distribution of biomass
521 throughout the nodules, despite deterministic factors, such as light and water, affecting the distribution
522 of specific microbial taxa, suggests that the carrying capacity of each niche inside the nodule might
523 be dependent on structural features of the substrate. As discussed above, the interior of the nodules is
524 far from being homogeneous; instead, the salt matrix harbors channels, elongated pores, and cavities
525 that are the result of salt dissolution and regular water movement (Artieda et al., 2015). This so-called
526 architecture of the substrate, which can be difficult to quantify in halite nodules, has been reported in
527 many other lithic microbiomes to have a great impact on endolithic microbial colonization (Walker
528 and Pace, 2007; Meslier et al., 2018).

529 While we identified notable differences in community composition between the nodule core
530 and peripheral positions, these differences were relatively subtle compared to those observed at larger
531 distance scales. This highlights the importance of water availability as a key factor governing
532 community composition, however, this could also imply increased rates of dispersion at the intra-
533 nodule distance scales. A way dispersion might be increased inside nodules is via liquid water
534 movement as a result of hydration cycles (Artieda et al., 2015). As the nodule gradually dehydrates
535 throughout the day, water is drawn toward the surface through capillary movement; during the night,
536 as the nodule re-hydrates, water is then drawn toward the center of the nodule (Davila et al., 2008;

537 Davila et al., 2013). This displacement not only drives the formation of the complex salt formations
538 observed in the halite nodules, but might also result in the mixing of the interior microbiota over
539 time. This idea is supported by the respective community composition at the sampled positions
540 within the nodules, which changed predictably along the vertical component in response to a
541 humidity gradient but changed seemingly randomly along the horizontal component. The difference
542 in physical isolation along the two axes is possibly explained by the regular water movements
543 between the halite core and periphery in response to the diel hydration cycles (Davila et al., 2008;
544 Davila et al., 2013). This displacement of water from the inside to the outside of the nodules is also
545 evidenced by the accumulation of scytonemin, a natural pigment produced by *Cyanobacteria*, at the
546 surface of halite nodules (Vitek et al., 2014).

547 Taken together, our findings on halite microbiomes suggest that progressively smaller scales
548 of diversity become less dependent on stochastic processes. This observation is in contrast with
549 existing research in soil, with more evenly distributed microbiomes, where it has been reported that
550 stochastic processes dictate assembly at smaller (centimeters) scales, while deterministic factors have
551 the largest impact on community assembly at larger distance scales (Shi et al., 2018; Zhao et al.,
552 2019). On the other hand, our findings are consistent within the framework of existing research in
553 systems with non-linear segregation such as gut microbiomes. Differences in gut microbiota between
554 individuals is driven by a combination of deterministic (e.g. diet) and neutral (stochastic colonization
555 and community drift) processes, but differences between colonization of intestine regions are not
556 dispersion-limited, and thus governed by deterministic factors (e.g. nutrient availability) (Albenberg
557 et al., 2014; Li and Ma, 2016; Jha et al., 2018). Similarly, the dispersion limitation in endolithic
558 microbiomes results in a non-linear relationship between distance and community similarity. Inter-
559 site community variability (regional and landscape distance scales in this study) likely follows a
560 distance-based model for community differentiation, whereby the composition of microbial
561 communities diverges with increasing distance (Allison and Martiny, 2008; Vellend, 2010).
562 However, our sampling scheme did not allow us to assess the relative contributions of environmental
563 conditions and distance on the changes in microbial community composition.

564 In this study, we found that water, light, and community drift impact microbiome assembly
565 differently at different distance scales, with higher rates of cell dispersion at the smaller scales
566 resulting in a more homogenous composition. While the study focused on general taxonomic
567 composition differences across spatial scales, differences in adaptations are likely to be more
568 pronounced at the functional level, which could be elucidated in a future shotgun metagenomics
569 study determining what gene and pathway are enriched in response to environmental differences.
570 Furthermore, previous research revealed that the microbial communities in separate halite nodules

571 converge at the functional potential level but diverge at the metatranscriptomic level (Uritskiy et al.,
572 2019b), indicating that investigating real-time transcriptional adaptations of these communities is
573 essential to understand their functioning and adaptations to these extreme conditions.

In review

574 **Tables and Figure Legends**

575 Table 1: Overview of the study design.

576

Scale	Distances	Distances	Condition differences
Regional	North and South sides of the salar	~20km	Microbiomes subject to different climate regimes
Landscape	Top and bottom of a hill	~300m	Microbiomes subject to slightly different local climates
Local	Inter-halite differences at the same site	~10m	Microbiomes in segregated and structurally unique nodules
Community	Intra-halite differences in the same nodule	~10cm	Micro-niches in the same halite, with varying light transmission patterns depending on position

577

578 Fig. 1: (A) Google Earth view of the Salar Grande with the North and South sampling regions. (B)
 579 Drone image of the hill at the North site showing the sampling areas at the top and bottom of the hill
 580 (photo by Mathias Meier). (C) Halite nodules at the top of the North hill. (D) Cross-section of a halite
 581 nodule with the locations of samples taken from the top, middle, and bottom of the nodule with
 582 respect to its original orientation in the field.

583

584 Fig. 2: Daily average over a year (March 25, 2019 to March 11, 2020) of temperature (A, B, C) and
 585 relative humidity (D, E, F) at North-Top sampling location inside three halite nodules (columns).
 586 Data were collected with separate HOBO sensors 1m above the ground (“Air”) or sealed inside a
 587 halite nodule near the top, middle, and bottom of the nodule. Highlight lines represent non-
 588 parametric polynomial kernel regression ($q=6$) with pyqt_fit.

589

590 Fig. 3: PCoA of Weighted Unifrac dissimilarity matrix of 16S rRNA gene amplicon sequences,
 591 comparing community compositions in samples from different sampling locations. A: samples from
 592 North and South sites (difference is significant, PERMANOVA: $pval<0.001$, test statistic= 28.36). B:
 593 samples from North-top and North-bottom (difference is significant, PERMANOVA: $pval= 0.001$,
 594 test statistic= 22.5). C: samples from the top, middle, and bottom positions within the halite nodules
 595 (note that the scatterplot projections show the third and fourth principal components). D: same as C
 596 but colored by the sample’s distance to the nodule’s surface (distance in cm encoded in colormap).

597

598 Fig. 4: Phylum-level taxonomy composition of halite communities from different locations. (A)
 599 North and South ends of the salar and (B) the top and bottom of the North hill. Relative abundances

600 were estimated with the Qiime2 taxonomy assignment pipeline. Only the six most abundant phyla
601 found in this community are shown.

602

603 Fig. 5: Relative abundance of major halite microbiome phyla inside the halite nodules at the top,
604 middle, and bottom positions within each sampled nodule slice. The relative abundances were
605 standardized to the average abundance of that phyla in each slice. Chlorophyta (chloroplast)
606 sequences were only detected at low abundances in a few samples, and are not shown here. Bars
607 above each phyla represent Student's t-test significance, and the stars denote the associated p-value
608 (***: pval<0.0001, **: pval<0.001, *: pval<0.01).

609

610 Fig. 6: Bray-Curtis dissimilarity between microbial communities in halite samples from different
611 sites, compared across distance scales: ~3 cm (samples from the same nodule and position along the
612 horizontal or vertical component), ~10 cm (samples from the same nodule at any internal position),
613 ~10 m (samples from different nodules at North-top), ~300 m (North-top vs North-bottom), and ~20
614 km (North vs South ends of the salar). Boxplots contain the dissimilarity between all possible inter-
615 sample comparisons in the considered sample groups. Stars denote the p-values of pairwise Student's
616 T-tests: p<0.05 (*), p<0.01 (**), p<0.001 (***).

617

618 **Conflict of Interest**

619 The authors declare that the research was conducted in the absence of any commercial or financial
620 relationships that could be construed as a potential conflict of interest.

621

622 **Author Contributions**

623 GU, JT, and JD conceived and oversaw the study; GU, DG, AD, and JD collected in-field samples
624 and metadata; GU, AM, MD, and SG processed field samples and constructed sequencing libraries;
625 PM collected and analyzed light spectra; GU processed and analyzed the data and wrote the
626 manuscript; AD, JT, PM, and JD edited the manuscript.

627

628 **Funding**

629 This work was funded by grants NNX15AP18G and 18-EXO18-0091 from NASA and DEB1556574
630 from the NSF.

631

632 **Acknowledgments**

633 We thank Mathias Meier for capturing areal drone footage of the sampling area, Victoria Meslier for
634 help in sample collection, and Brian Glass for organizing field expeditions.

635

636 **Data Availability Statement**

637 All raw amplicon sequencing data used in this study is publicly available through NCBI Sequence
638 Read Archive under project ID PRJNA641398. All processing pipelines, figure-making scripts, and
639 intermediate data is publicly available on https://github.com/ursky/spatial_paper.

640

641

642 **References**

- 643 Albenberg, L., Esipova, T.V., Judge, C.P., Bittinger, K., Chen, J., Laughlin, A., et al. (2014).
 644 Correlation between intraluminal oxygen gradient and radial partitioning of intestinal
 645 microbiota. *Gastroenterology* 147, 1055-1063 e1058. doi: 10.1053/j.gastro.2014.07.020.
- 646 Allison, S.D., and Martiny, J.B. (2008). Colloquium paper: resistance, resilience, and redundancy in
 647 microbial communities. *Proc. Natl. Acad. Sci. U.S.A.* 105, 11512-11519.
- 648 Armstrong, A., Valverde, A., Ramond, J.B., Makhalanyane, T.P., Jansson, J.K., Hopkins, D.W., et al.
 649 (2016). Temporal dynamics of hot desert microbial communities reveal structural and
 650 functional responses to water input. *Sci. Rep.* 6, 34434. doi: 10.1038/srep34434.
- 651 Artieda, O., Davila, A., Wierzchos, J., Buhler, P., Rodríguez-Ochoa, R., Pueyo, J., et al. (2015).
 652 Surface evolution of salt-encrusted playas under extreme and continued dryness. *Earth Surf.
 653 Proc. Landf.* 40, 1939-1950.
- 654 Bolyen, E., Rideout, J.R., Dillon, M.R., Bokulich, N.A., Abnet, C.C., Al-Ghalith, G.A., et al.
 655 (2019a). Author Correction: Reproducible, interactive, scalable and extensible microbiome
 656 data science using QIIME 2. *Nat. Biotechnol.* 37, 1091. doi: 10.1038/s41587-019-0252-6.
- 657 Bolyen, E., Rideout, J.R., Dillon, M.R., Bokulich, N.A., Abnet, C.C., Al-Ghalith, G.A., et al.
 658 (2019b). Reproducible, interactive, scalable and extensible microbiome data science using
 659 QIIME 2. *Nat. Biotechnol.* 37, 852-857.
- 660 Cáceres, L., Gómez-Silva, B., Garró, X., Rodríguez, V., Monardes, V., and McKay, C.P. (2007).
 661 Relative humidity patterns and fog water precipitation in the Atacama Desert and biological
 662 implications. *Journ. of Geoph. Res.: Biogeos.* 112, G4. doi: 10.1029/2006jg000344.
- 663 Callahan, B.J., McMurdie, P.J., Rosen, M.J., Han, A.W., Johnson, A.J., and Holmes, S.P. (2016).
 664 DADA2: High-resolution sample inference from Illumina amplicon data. *Nat. Methods* 13,
 665 581-583.
- 666 Carreira, C., Piel, T., Staat, M., Stuut, J.B., Middelboe, M., and Brussaard, C.P. (2015). Microscale
 667 spatial distributions of microbes and viruses in intertidal photosynthetic microbial mats.
 668 *Springerplus* 4, 239. doi: 10.1186/s40064-015-0977-8.
- 669 Caruso, T., Chan, Y., Lacap, D.C., Lau, M.C., McKay, C.P., and Pointing, S.B. (2011). Stochastic
 670 and deterministic processes interact in the assembly of desert microbial communities on a
 671 global scale. *ISME J.* 5, 1406-1413.

- 672 Cereceda, P., Larrain, H., Osses, P., Farías, M., and Egaña, I. (2008). The spatial and temporal
673 variability of fog and its relation to fog oases in the Atacama Desert, Chile. *Atmospheric Res.*
674 87, 312-323.
- 675 Crits-Christoph, A., Gelsinger, D.R., Ma, B., Wierzchos, J., Ravel, J., Davila, A., et al. (2016).
676 Functional interactions of archaea, bacteria and viruses in a hypersaline endolithic
677 community. *Environ. Microbiol.* 18, 2064-2077.
- 678 Crits-Christoph, A., Robinson, C.K., Barnum, T., Fricke, W.F., Davila, A.F., Jedynak, B., et al.
679 (2013). Colonization patterns of soil microbial communities in the Atacama Desert.
680 *Microbiome* 1, 28. doi: 10.1186/2049-2618-1-28.
- 681 Davila, A.F., Gomez-Silva, B., de los Rios, A., Ascaso, C., Olivares, H., McKay, C.P., et al. (2008).
682 Facilitation of endolithic microbial survival in the hyperarid core of the Atacama Desert by
683 mineral deliquescence. *J. Geophys. Res.* 113, G01028. doi:01010.01029/02007JG000561.
- 684 Davila, A.F., Hawes, I., Ascaso, C., and Wierzchos, J. (2013). Salt deliquescence drives
685 photosynthesis in the hyperarid Atacama Desert. *Environ. Microbial. Rep.* 5, 583–587.
- 686 Davila, A.F., Hawes, I., Garcia, J., Gelsinger, D.R., DiRuggiero, J., Ascaso, C., et al. (2015). In situ
687 metabolism in halite endolithic microbial communities of the hyperarid Atacama Desert.
688 *Front. Microbiol.* 6,103. [doi: 10.3389/fmicb.2015.01035](https://doi.org/10.3389/fmicb.2015.01035).
- 689 Davila, A.F., Warren-Rhodes, K., and J. DiRuggiero. “*The Atacama Desert: A Window into Late
690 Mars Habitability?*” in Martian Geological Enigmas. Eds R. Soare, S. Conway, P. Williams,
691 and D. Oehler (Elsevier), in press.
- 692 Evans, S., Martiny, J.B., and Allison, S.D. (2017). Effects of dispersal and selection on stochastic
693 assembly in microbial communities. *ISME J.* 11, 176-185.
- 694 Feeser, K.L., Van Horn, D.J., Buelow, H.N., Colman, D.R., McHugh, T.A., Okie, J.G., et al. (2018).
695 Local and Regional Scale Heterogeneity Drive Bacterial Community Diversity and
696 Composition in a Polar Desert. *Front. Microbiol.* 9, 1928. doi: 10.3389/fmicb.2018.01928.
- 697 Finstad, K., Pfeiffer, M., McNicol, G., Barnes, J., Demergasso, C., Chong, G., et al. (2016). Rates
698 and geochemical processes of soil and salt crust formation in Salars of the Atacama Desert,
699 Chile. *Geoderma* 284, 57-72.
- 700 Finstad, K.M., Probst, A.J., Thomas, B.C., Andersen, G.L., Demergasso, C., Echeverria, A., et al.
701 (2017). Microbial Community Structure and the Persistence of Cyanobacterial Populations in

- 702 Salt Crusts of the Hyperarid Atacama Desert from Genome-Resolved Metagenomics. *Front.*
703 *Microbiol.* 8, 1435. doi: 10.3389/fmicb.2017.01435.
- 704 Frossard, A., Ramond, J.B., Seely, M., and Cowan, D.A. (2015). Water regime history drives
705 responses of soil Namib Desert microbial communities to wetting events. *Sci. Rep.* 5, 12263.
706 doi: 10.1038/srep12263.
- 707 Gelsinger, D.R., Uritskiy, G., Reddy, R., Munn, A., Farney, K., and DiRuggiero, J. (2020).
708 Regulatory Noncoding Small RNAs Are Diverse and Abundant in an Extremophilic
709 Microbial Community. *mSystems* 5:e00584-19. doi: 10.1128/mSystems.00584-19.
- 710 Goldford, J.E., Lu, N., Bajic, D., Estrela, S., Tikhonov, M., Sanchez-Gorostiaga, A., et al. (2018).
711 Emergent simplicity in microbial community assembly. *Science* 361, 469-474.
- 712 Green, J.L., Bohannan, B.J., and Whitaker, R.J. (2008). Microbial biogeography: from taxonomy to
713 traits. *Science* 320, 1039-1043.
- 714 Gunde-Cimerman, N., Plemenitas, A., and Oren, A. (2018). Strategies of adaptation of
715 microorganisms of the three domains of life to high salt concentrations. *FEMS Microbiol.*
716 *Rev.* 42,353-375.
- 717 Hamm, J.N., Erdmann, S., Eloë-Fadrosh, E.A., Angeloni, A., Zhong, L., Brownlee, C., et al. (2019).
718 Unexpected host dependency of Antarctic Nanohaloarchaeota. *Proc. Natl. Acad. Sci. U. S. A.*
719 116, 14661-14670.
- 720 Jha, A.R., Davenport, E.R., Gautam, Y., Bhandari, D., Tandukar, S., Ng, K.M., et al. (2018). Gut
721 microbiome transition across a lifestyle gradient in Himalaya. *PLoS Biol.* 16, e2005396. doi:
722 10.1371/journal.pbio.2005396.
- 723 Kepner, R.L., and Pratt, J.R. (1994). Use of fluorochromes for direct enumeration of total bacteria in
724 environmental samples: Past and present. *Microb. Rev.* 58, 603-615.
- 725 Li, L., and Ma, Z.S. (2016). Testing the Neutral Theory of Biodiversity with Human Microbiome
726 Datasets. *Sci. Rep.* 6, 31448. doi: 10.1038/srep31448.
- 727 Mandakovic, D., Rojas, C., Maldonado, J., Latorre, M., Travisany, D., Delage, E., et al. (2018).
728 Structure and co-occurrence patterns in microbial communities under acute environmental
729 stress reveal ecological factors fostering resilience. *Sci. Rep.* 8, 5875. doi: 10.1038/s41598-
730 018-23931-0.

- 731 Mandal, S., Van Treuren, W., White, R.A., Eggesbo, M., Knight, R., and Peddada, S.D. (2015).
 732 Analysis of composition of microbiomes: a novel method for studying microbial composition.
 733 *Microb. Ecol. Health Dis.* 26, 27663. doi: 10.3402/mehd.v26.27663.
- 734 Mello, B.L., Alessi, A.M., McQueen-Mason, S., Bruce, N.C., and Polikarpov, I. (2016). Nutrient
 735 availability shapes the microbial community structure in sugarcane bagasse compost-derived
 736 consortia. *Sci. Rep.* 6, 38781. doi: 10.1038/srep38781.
- 737 Merino, N., Aronson, H.S., Bojanova, D.P., Feyhl-Buska, J., Wong, M.L., Zhang, S., et al. (2019).
 738 Living at the Extremes: Extremophiles and the Limits of Life in a Planetary Context. *Front.*
 739 *Microbiol.* 10, 780. doi: 10.3389/fmicb.2019.00780.
- 740 Meslier, V., Casero, M.C., Dailey, M., Wierzchos, J., Ascaso, C., Artieda, O., et al. (2018).
 741 Fundamental drivers for endolithic microbial community assemblies in the hyperarid
 742 Atacama Desert. *Environ. Microbiol.* 20, 1765-1781.
- 743 Narasingarao, P., Podell, S., Ugalde, J.A., Brochier-Armanet, C., Emerson, J.B., Brocks, J.J., et al.
 744 (2012). De novo metagenomic assembly reveals abundant novel major lineage of Archaea in
 745 hypersaline microbial communities. *ISME J.* 6, 81-93. .
- 746 Needham, D.M., and Fuhrman, J.A. (2016). Pronounced daily succession of phytoplankton, archaea
 747 and bacteria following a spring bloom. *Nat. Microbiol.* 1, 16005. doi:
 748 10.1038/nmicrobiol.2016.5.
- 749 Nemergut, D.R., Schmidt, S.K., Fukami, T., O'Neill, S.P., Bilinski, T.M., Stanish, L.F., et al. (2013).
 750 Patterns and processes of microbial community assembly. *Microbiol. Mol. Biol. Rev.* 77, 342-
 751 356.
- 752 Nienow, J.A.C., McKay, C.P., and Friedmann, E.I. (1988). The cryptoendolithic microbial
 753 environment in the Ross desert of Antarctica: light in the photosynthetically active region.
 754 *Microb. Ecol.* 16, 271-289.
- 755 Nishida, A., Thiel, V., Nakagawa, M., Ayukawa, S., and Yamamura, M. (2018). Effect of light
 756 wavelength on hot spring microbial mat biodiversity. *PLoS One* 13 e0191650. doi:
 757 10.1371/journal.pone.0191650.
- 758 Oren, A. (2008). Microbial life at high salt concentrations: phylogenetic and metabolic diversity.
 759 *Saline Systems* 4, 2. doi:10.1186/1746-1448-1184-1182.
- 760 Oren, A. (2014). Halophilic archaea on Earth and in space: growth and survival under extreme
 761 conditions. *Philos. Trans. A Math Phys Eng. Sci.* 372, 2030. doi: 10.1098/rsta.2014.0194.

- 762 Quast, C., Pruesse, E., Yilmaz, P., Gerken, J., Schweer, T., Yarza, P., et al. (2013). The SILVA
763 ribosomal RNA gene database project: improved data processing and web-based tools.
764 *Nucleic Acids Res.* 41, D590-596. doi: 10.1093/nar/gks1219.
- 765 Robinson, C.K., Wierzchos, J., Black, C., Crits-Christoph, A., Ma, B., Ravel, J., et al. (2015).
766 Microbial diversity and the presence of algae in halite endolithic communities are correlated
767 to atmospheric moisture in the hyper-arid zone of the Atacama Desert. *Environ. Microbiol.*
768 17, 299-315.
- 769 Rocha, E.P.C. (2018). Neutral Theory, Microbial Practice: Challenges in Bacterial Population
770 Genetics. *Mol. Biol. Evol.* 35:6, 1338-1347..
- 771 Schmid, A.K., Allers, T., and DiRuggiero, J. (2020). SnapShot: Microbial Extremophiles. *Cell* 180,
772 818-818 e811.
- 773 Seyedkarimi, M.S., Aramvash, A., and Ramezani, R. (2015). High production of bacteriorhodopsin
774 from wild type Halobacterium salinarum. *Extremophiles* 19, 1021-1028.
- 775 Shi, Y., Li, Y., Xiang, X., Sun, R., Yang, T., He, D., et al. (2018). Spatial scale affects the relative
776 role of stochasticity versus determinism in soil bacterial communities in wheat fields across
777 the North China Plain. *Microbiome* 6, 27. doi: 10.1186/s40168-018-0409-4.
- 778 Sigliocco, A., Paiardini, A., Piscitelli, M., and Pascarella, S. (2011). Structural adaptation of
779 extreme halophilic proteins through decrease of conserved hydrophobic contact surface. *BMC*
780 *Struc.t Biol.* 11, 50. doi: 10.1186/1472-6807-11-50.
- 781 Tucker, C.M., Cadotte, M.W., Carvalho, S.B., Davies, T.J., Ferrier, S., Fritz, S.A., et al. (2017). A
782 guide to phylogenetic metrics for conservation, community ecology and macroecology. *Biol.*
783 *Rev. Camb. Philos. Soc.* 92, 698-715. doi: 10.1111/brv.12252.
- 784 Uritskiy, G., Getsin, S., Munn, A., Gomez-Silva, B., Davila, A., Glass, B., et al. (2019a). Halophilic
785 microbial community compositional shift after a rare rainfall in the Atacama Desert. *ISME J.*
786 13, 2737–2749.
- 787 Uritskiy, G., Tisza, M.J., Gelsinger, D.R., Munn, A., Taylor, J., and DiRuggiero, J. (2019b). Cellular
788 life from the three domains and viruses are transcriptionally active in a hypersaline desert
789 community. *bioRxiv*, 839134. doi: 10.1101/839134.
- 790 Vellend, M. (2010). Conceptual synthesis in community ecology. *Q. Rev. Biol.* 85, 183-206.

- 791 Vitek, P., Jehlicka, J., Ascaso, C., Masek, V., Gomez-Silva, B., Olivares, H., et al. (2014).
792 Distribution of scytonemin in endolithic microbial communities from halite crusts in the
793 hyperarid zone of the Atacama Desert, Chile. *FEMS Microbiol. Ecol.* 90, 351-366.
- 794 Walker, J.J., and Pace, N.R. (2007). Endolithic microbial ecosystems. *Annu. Rev. Microbiol.* 61, 331-
795 347.
- 796 Wierzchos, J., Ascaso, C., and McKay, C.P. (2006). Endolithic cyanobacteria in halite rocks from the
797 hyperarid core of the Atacama Desert. *Astrobiology* 6, 415-422.
- 798 Wierzchos, J., de los Ríos, A., and Ascaso, C. (2012). Microorganisms in desert rocks: the edge of
799 life on Earth. *Inter. Microbiol.* 15, 173-183.
- 800 Wierzchos, J., DiRuggiero, J., Vítek, P., Artieda, O., Souza-Egipsy, V., Skaloud, P., et al. (2015).
801 Adaptation strategies of endolithic chlorophototrophs to survive the hyperarid and extreme
802 solar radiation environment of the Atacama Desert. *Front. Microbiol.* 6, 934. doi:
803 910.3389/fmicb.2015.00934.
- 804 Zhao, P., Bao, J., Wang, X., Liu, Y., Li, C., and Chai, B. (2019). Deterministic processes dominate
805 soil microbial community assembly in subalpine coniferous forests on the Loess Plateau.
806 *PeerJ* 7, e6746. doi: 10.7717/peerj.6746.

807

Figure 1.TIF

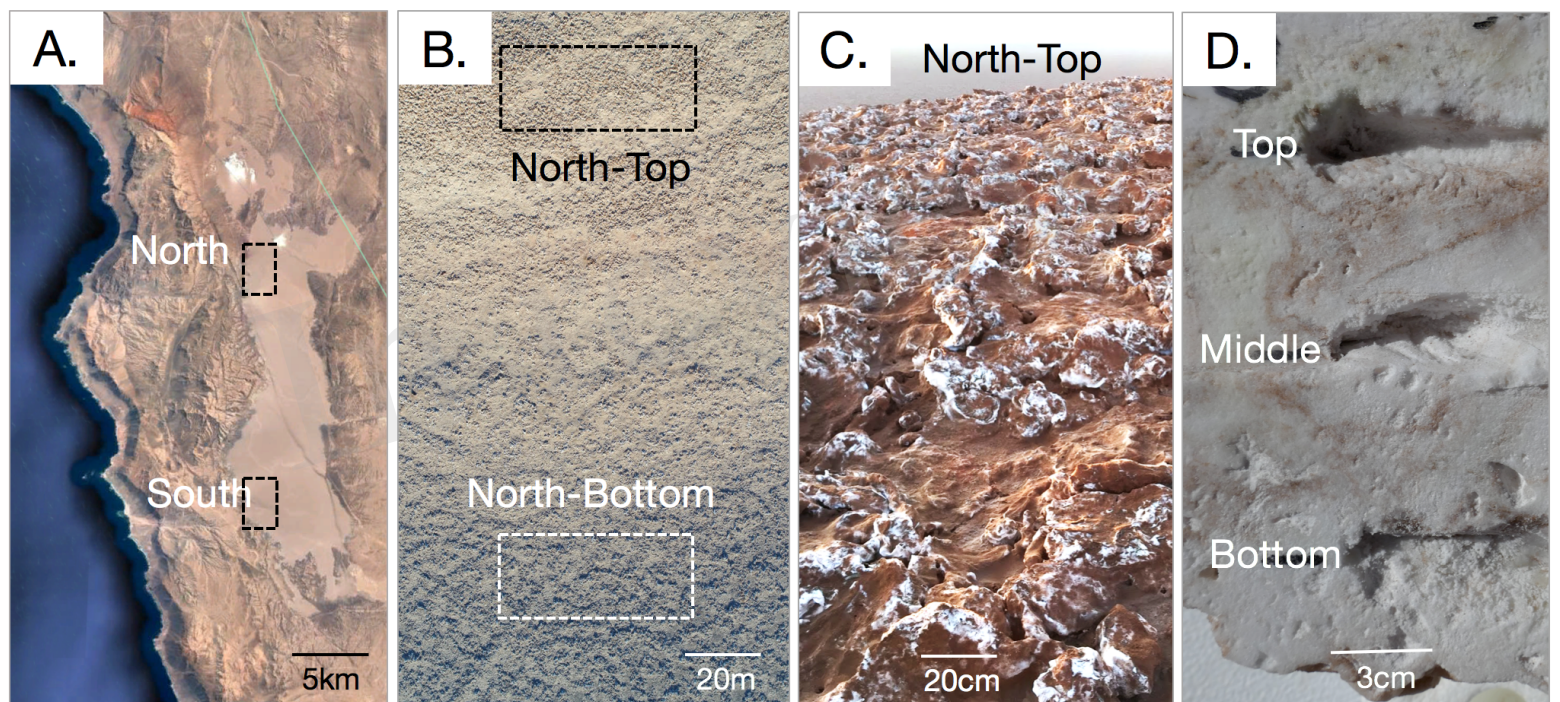


Figure 2.TIF

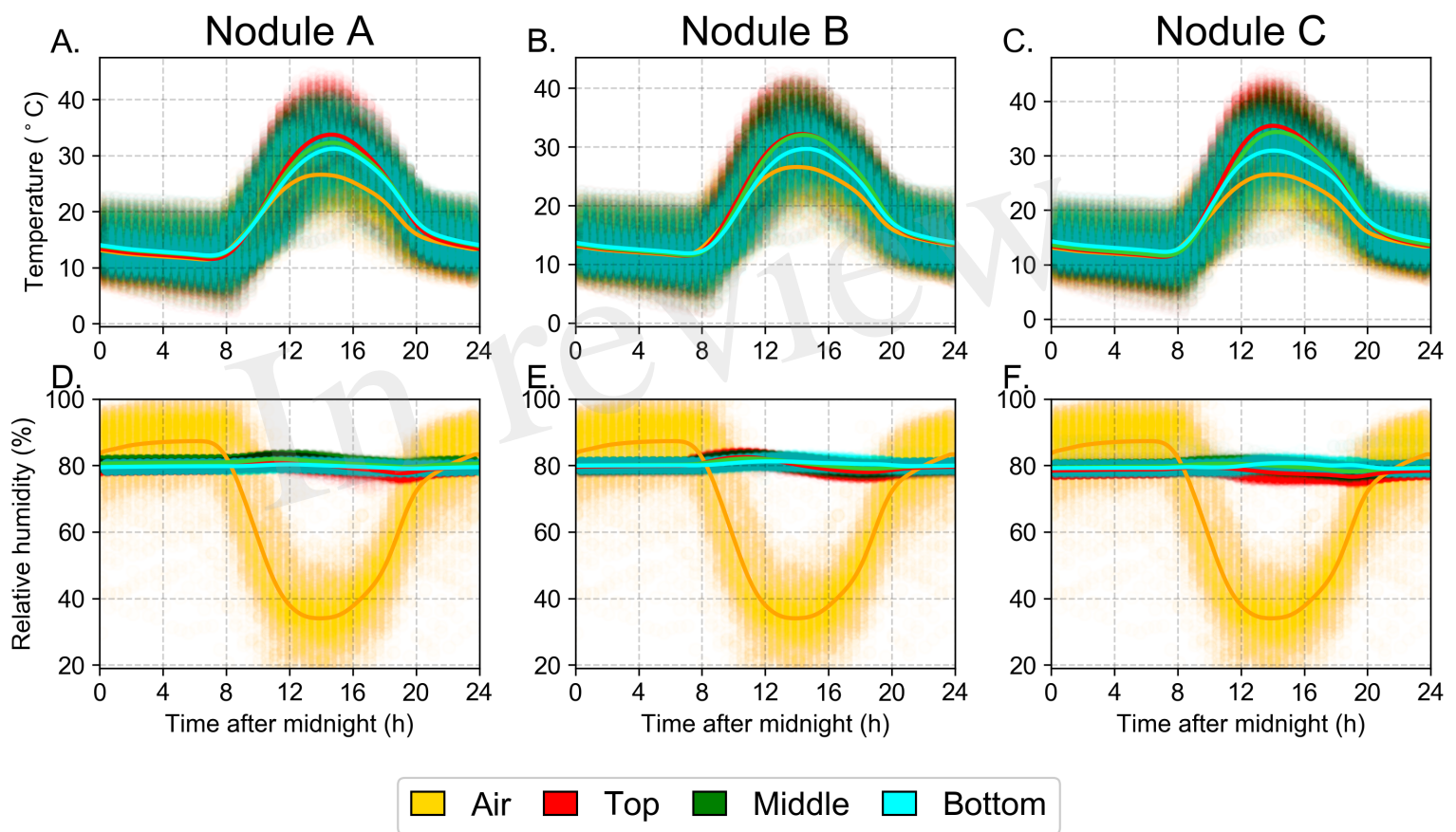


Figure 3.TIF

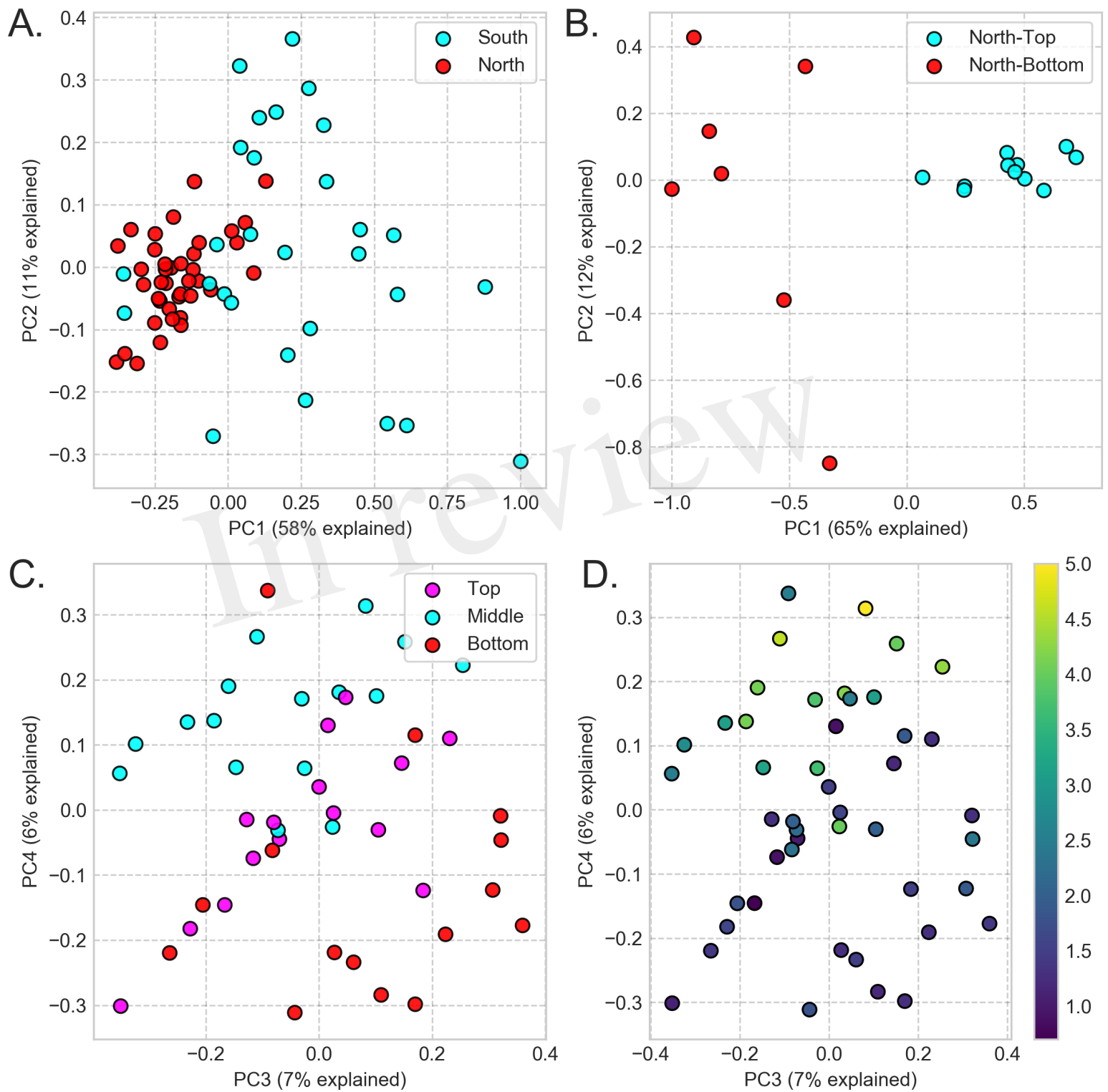


Figure 4.TIF

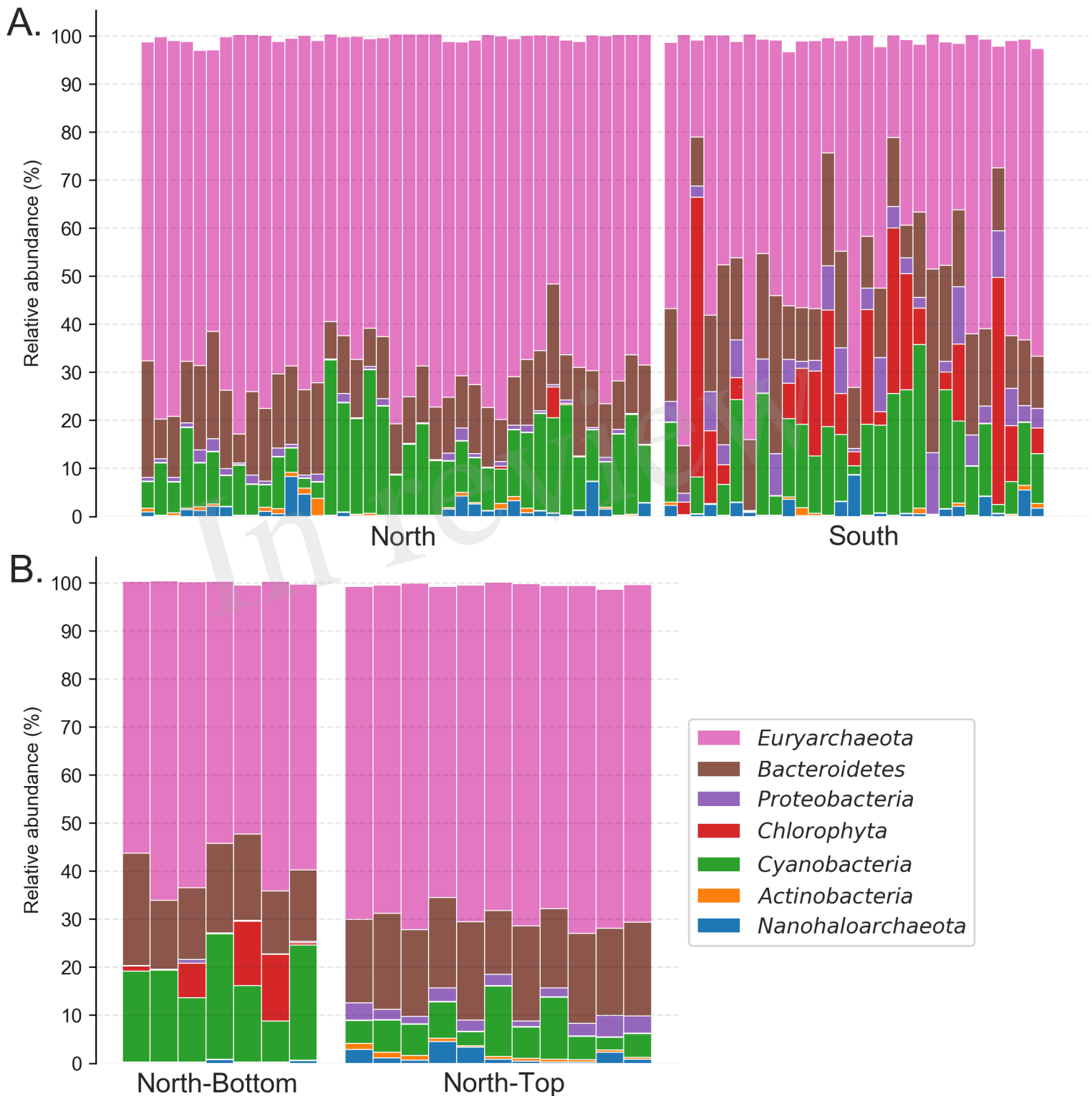


Figure 5.TIF

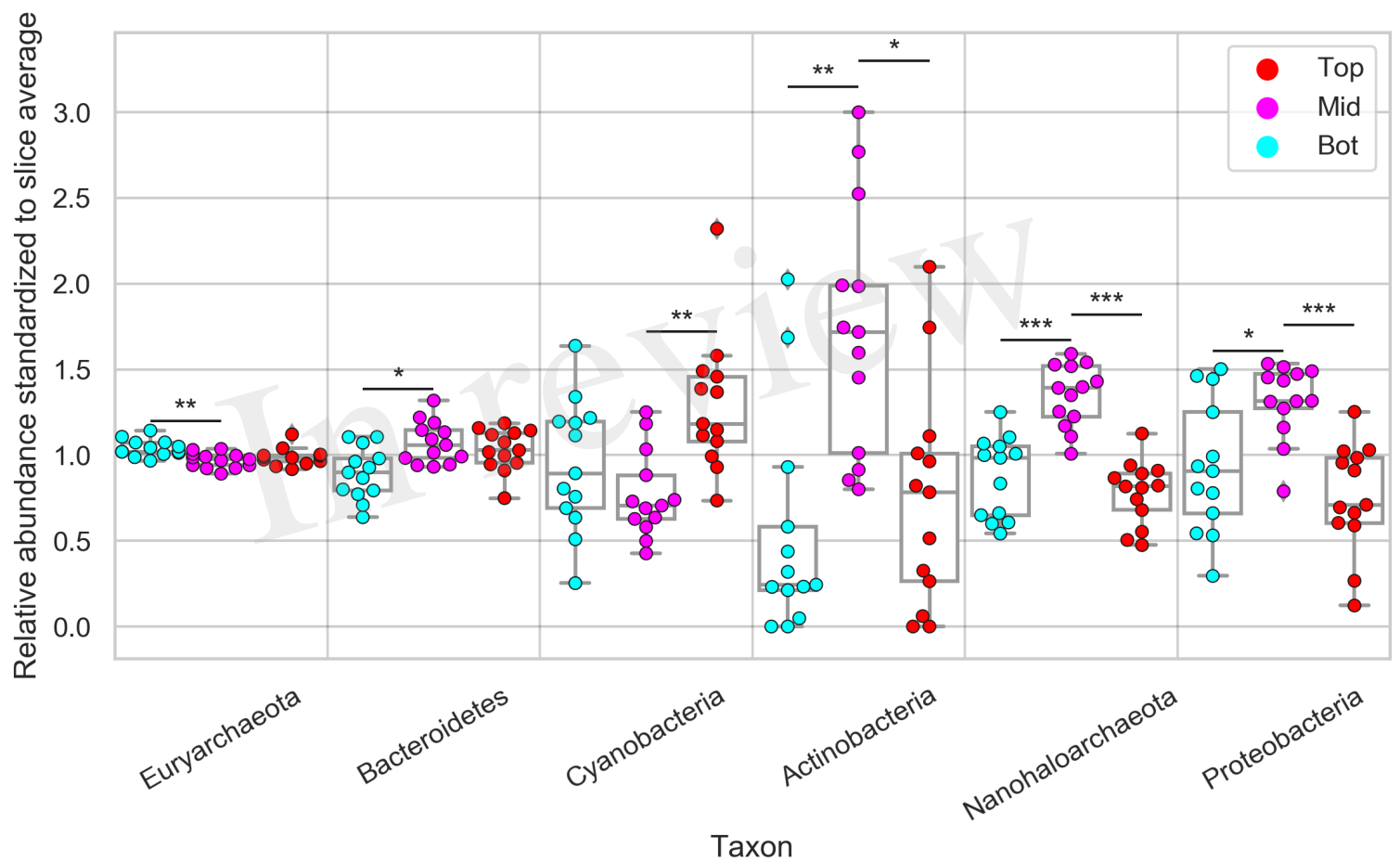


Figure 6.TIF

